Archives of Civil and Mechanical Engineering (2024) 24:22
https://doi.org/10.1007/s43452-023-00819-z

ORIGINAL ARTICLE

Vibration response of a hybrid steel–timber building element with uncertain material and joint parameters

Bettina Chocholaty[1] · Martin Eser[1] · Karl-Alexander Hoppe[1] · Daotong Wang[1] · Steffen Marburg[1]

Received: 26 August 2023 / Revised: 2 October 2023 / Accepted: 22 October 2023 / Published online: 18 December 2023
© The Author(s) 2023

Abstract
The design of building elements is usually done conservatively by considering safety factors. However, more efficient designs are gaining interest for economic and sustainability reasons. Hence, an adequate prediction tool can improve the design of building elements. Probabilistic modeling, for example, Monte Carlo simulations, represents a remedy to this by examining uncertainties in a structure through uncertain input parameters. In this work, a Monte Carlo simulation is performed to quantify the uncertainty in the modal properties of a hybrid steel–timber building element. The material properties of the timber material and the stiffness of the structural joints are considered uncertain inputs. The probabilistic properties of the timber material are evaluated utilizing Bayesian inference instead of the usually applied empirical methods. Using these inferred timber material properties leads to a good match of simulated and measured natural frequencies of the timber components. These parameters are utilized together with the joints' uncertain inputs in the Monte Carlo simulation of the hybrid steel–timber building element. The results show a significant span for the identified eigenfrequencies, which proves the relevance of probabilistic analyses for the vibration characteristics of building elements.

Keywords Hybrid steel–timber elements · Monte Carlo simulation · Vibrations · Bayesian inference

1 Introduction

Hybrid wood structures combined with steel or concrete are moving into the focus of wood construction research, especially in the topic of vibrations [1]. Human activities, e.g., walking or jogging, can significantly influence the design of hybrid steel–timber floor elements in terms of vibrations [2]. In the design process of floor structures related to vibrations, calculations or certified measurements are required [3]. However, analytical calculations become challenging for complex cross-sections, emphasizing the need to develop reliable, advanced prediction tools for vibrations of compounded structures, such as hybrid steel–timber building elements. These predictive models prove to be relevant, especially for material-efficient designs in the context of economic efficiency and sustainability, since without predictive tools, various prototypes have to be tested experimentally [4].

The vibroacoustic behavior of hybrid steel–timber floors has already been studied experimentally and numerically [2, 5, 6]. A steel–timber beam made of a Cross-Laminated-Timber (CLT) panel and an H-shaped steel profile has been investigated concerning natural frequencies, mode shapes, modal damping ratios, and acceleration response. A finite element (FE) model has been updated to match the results from experimental analyses [6]. The same structure has been analyzed concerning vibration serviceability in [2]. A different structure has been studied in [5]. Here, the authors have investigated the vibrational behavior of a structure made of top and bottom laminated veneer lumber (LVL) panels and a trapezoidal steel web.

In practice, the response prediction of a vibroacoustic system is generally performed through mechanical modeling, which introduces data and model uncertainties. Model uncertainties relate to the applicability of a model to the specific problem at hand and represent a type of epistemic error. On the other hand, data uncertainties constitute a type of aleatoric error and are related to the parameters of a

✉ Bettina Chocholaty
bettina.chocholaty@tum.de

[1] Chair of Vibroacoustics of Vehicles and Machines, Department of Engineering Physics and Computation, TUM School of Engineering and Design, Technical University of Munich, Boltzmannstraße 15, 85748 Garching bei München, Germany

system, e.g., geometrical parameters, boundary conditions, or material properties. Data uncertainties can be considered by using random quantities, e.g., random variables or stochastic fields, for the parameters in the prediction tool [7, 8]. However, in engineering practice, those uncertainties are often accounted for through safety factors [9] leading to conservative designs.

To develop more efficient designs, research on reliable predictions for building elements focuses increasingly on considering data uncertainties instead of safety factors. Recent studies on the stochastic analyses of wooden floors, i.e., a CLT slab [10] and a floor made of wood beams and particle boards [11], use the Monte Carlo (MC) method to include the randomness of the components' material properties and to determine the vibroacoustic response of the floor in confidence intervals. The random material parameter inputs are found by calibrating FE models to match eigenfrequencies from an experimental modal analysis. In [11], this has been done by determining the mean and standard deviation for the material parameters from 62 measurements on wooden beams. In [10], using a random elasticity tensor built from initial values from the literature, the best combination of material parameters in the FE model is sought to calibrate the model with results from an experimental modal analysis. Furthermore, non-Gaussian uncertain parameters of ash wood are identified using generalized polynomial chaos expansions and experimental modal data by solving a stochastic inverse problem in [12, 13].

Another approach to identifying unknown, uncertain parameters based on experiments and modeling is Bayesian inference. Former research has exploited Bayesian inference for laminated, orthotropic materials such as engineered wood products, i.e., for general thin orthotropic laminates [14], thick orthotropic laminated plates [15], laminated timber beams [16], and CLT [17]. The studies either use static deflection tests [16], simulated and experimentally determined natural frequencies [14, 15] or frequency response data of a linear dynamic model and measurements [17] to determine the material properties.

Prior investigations into the uncertainty quantification of building elements have predominantly relied on deterministic methods for identifying material properties through model calibration using experimental data [10, 11]. Alternatively, some studies have considered Bayesian inference to incorporate prior information on elastic constants, as exemplified by [15]. Notably, these Bayesian inference studies on engineered wood materials focus solely on inferring material properties without integrating them into subsequent analyses. Consequently, a critical gap emerges in connecting these approaches. In this study, this gap is filled by applying a novel combination of both methodologies to address the vibrational behavior of a hybrid steel-timber building element. This research concentrates on the quantification of uncertainty in the vibroacoustic behavior of this hybrid structure, focusing on the variability of modal properties. The approach adopted encompasses two main phases, detailed in Sect. 2 and Sect. 3. First, Bayesian inference is applied to establish probabilistic representations of timber material properties, incorporating the inherent variability found in real-world scenarios. These probabilistic representations serve as the foundation for the subsequent phase, where a probabilistic model is developed to predict the vibroacoustic response of the hybrid structure, as discussed in Sect. 3. The outcomes of these interconnected phases undergo thorough analysis and discussion in Sect. 4.

In summary, this article introduces a novel combination of two distinct methodologies applied for the first time to the examination of a hybrid steel–timber building element. This research contributes to the field of uncertainty quantification in vibrational behavior, yielding valuable insights into the dynamic variations of modal properties while leveraging more efficient structural designs.

2 Materials and methods

This study aims to quantify uncertainty for the vibroacoustic behavior of a hybrid steel–timber building element, which has been previously studied in terms of vibroacoustics in [5]. The variability of the natural frequencies of the element due to uncertain inputs is analyzed. The overall workflow is visualized in Fig. 1. In Sect. 2.1, the vibrational behavior of the hybrid steel–timber building element is evaluated experimentally and numerically. The stiffness of the joints and the material properties of the timber are assigned to be uncertain inputs. For the latter, the approach of Bayesian inference is applied to characterize the uncertainty in Sect. 2.2. For the former, the parameters are identified by maximum a posteriori (MAP) estimation, and their variation is based on literature references (Sect. 2.3). Finally, the numerical model and these uncertain inputs are used in a probabilistic analysis in Sect. 2.4.

2.1 Experimental and numerical investigations on the hybrid steel–timber element

The investigated hybrid structure utilizes LVL panels as top and bottom planking and a trapezoidal steel web. Fasteners connect the individual components. An overview of the concept is given in Fig. 1. The dimensions of the samples are depicted in Fig. 1 and listed in Table 1.

An FE model is created for the probabilistic analysis as described in Sect. 2.1.2 and is validated by vibration measurements (Sect. 2.1.1).

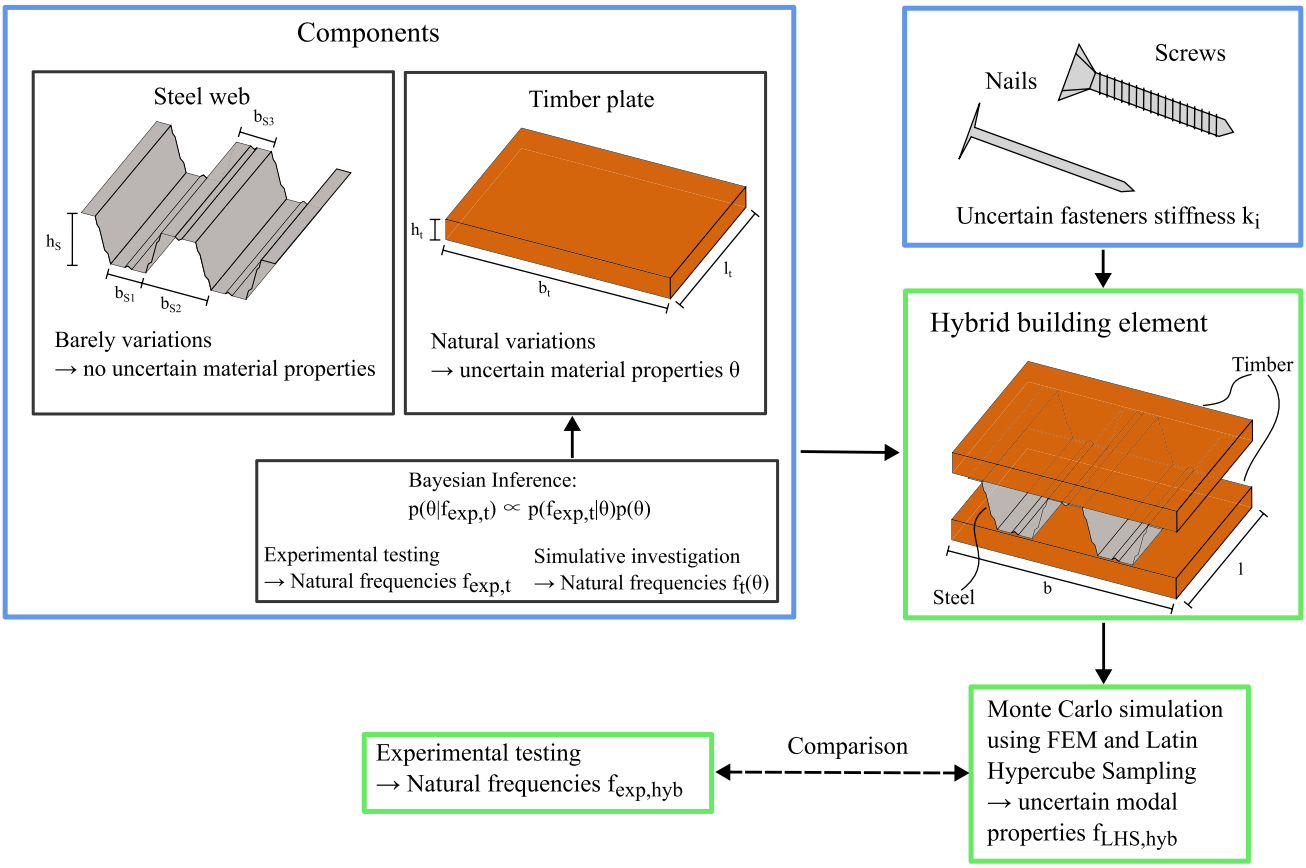

Fig. 1 Overview of methodological approach

Table 1 Geometric properties of the hybrid steel–timber test sample (refer to Fig. 1 for the parameter definition)

l [m]	b [m]	h_t [m]	d_s [m]	h_s [m]	b_{s1} [m]	b_{s2} [m]	b_{s3} [m]
3.5	0.900	0.039	$0.75 \cdot 10^{-3}$	0.155	0.110	0.170	0.04

2.1.1 Measurements on the hybrid element

The following paragraph briefly describes the measurement setup and procedure. More details are available in [5]. Measurements of vibration on the hybrid steel–timber element are carried out (Fig. 2). A B &K[1] modal exciter type 4284 applies a pseudo-random excitation on the structure by a stinger. Heavy-duty slings support the specimen. Hanging supports are chosen in the measurements to exclude influences from uncertain boundary conditions, since unconstrained supports are less challenging to realize adequately [18]. Furthermore, a B &K force transducer Deltatron Type 8230 measures the applied force. The vibrations of the specimens' surface are identified by a scanning Laser Doppler Vibrometer PSV-500 (LDV)[2] at an evenly distributed grid

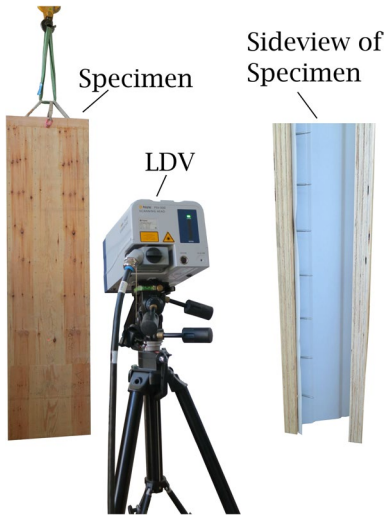

Fig. 2 Measurement setup for the hybrid element

[1] Hottinger Brüel & Kjær GmbH, D-64293 Darmstadt, Germany.

[2] Polytec GmbH, D-76337 Waldbronn, Germany.

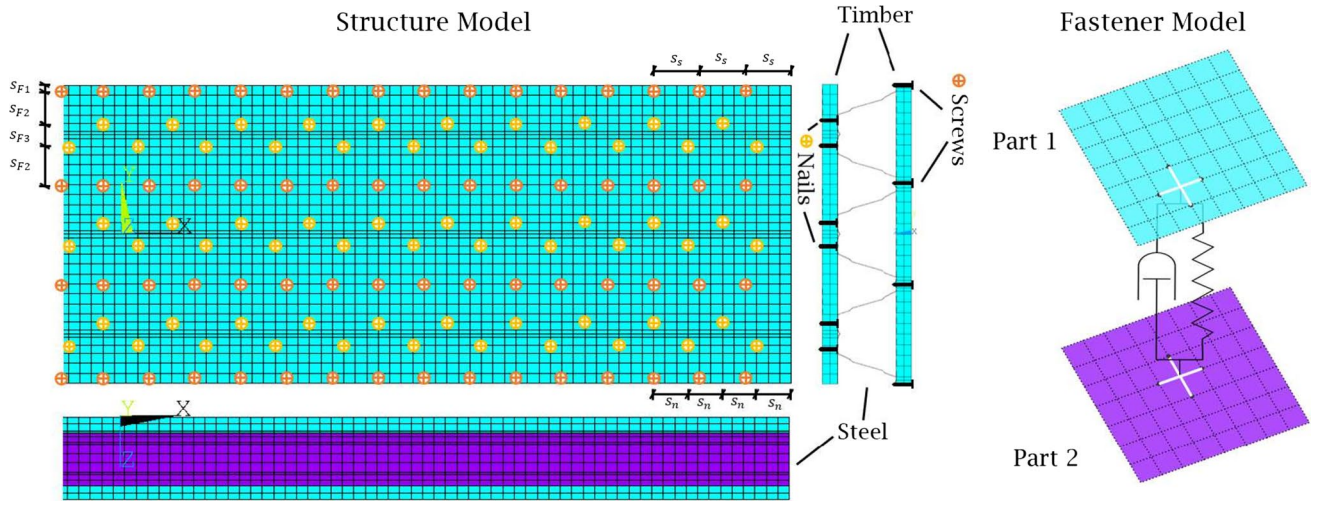

Fig. 3 Finite element model of the hybrid steel–timber element: structural model is depicted on the left and the fastener model on the right

of locations on the structure. For each scan point, a Fourier transform is utilized to transform the determined time data. Subsequently, the frequency response functions are calculated by means of the measured force and velocity signals. The Polytec system software applies a rectangular window to the signals.

The first five eigenfrequencies of the hybrid structure $f_{\text{exp,hyb}}$ are identified by an experimental modal analysis [18].

2.1.2 Finite element model

The commercial software ANSYS [19] is used to simulate the vibrational behavior of the hybrid structure. The FE representation of the steel–timber structure is visualized in Fig. 3. The lower and upper wooden panels are modeled by orthotropic and hexahedral elements (SOLID186) with quadratic shape functions. The steel web is meshed by isotropic, quadratic shell elements (SHELL281). The fasteners are simulated by parallel spring and damper elements (COMBIN14) applied for all translational degrees of freedom (DOFs) of nodes related to fasteners (as in, e.g., [20]). The adjacent nodes of a fastener are rigidly coupled in terms of translational DOFs (Fig. 3). In longitudinal direction, the screws are placed with $s_s = 0.12\,\text{m}$ and the nails with $s_n = 0.09\,\text{m}$. The transversal fastener distances are given as $s_{F1} = 0.010\,\text{m}$, $s_{F2} = 0.103\,\text{m}$ and $s_{F3} = 0.055\,\text{m}$. The used mesh size is approximately $l_{\text{ele}} = 0.03\,\text{m}$ for the timber components and $l_{\text{ele}} = 0.02\,\text{m}$ for the steel parts. Those element sizes are chosen as a good compromise between geometrical constraints and the rule of thumb to use six to eight quadratic elements per wavelength [21]. The boundary conditions in the simulations are modeled as free supports to adopt the measurement setup.

The influence of input parameter uncertainties on the natural frequencies of the building element is of interest. Therefore, modal analysis is conducted in ANSYS. The five structural mode shapes $f_{\text{FE,hyb}}$ matching the experimentally determined ones are computed.

The FE model uses material properties for the steel and timber components, as well as joint and geometric parameters as inputs. The geometrical inputs for the hybrid specimen are given in Table 1. Uncertainties from geometrical parameters are assumed to be negligible. Ballast [22] states manufacturing tolerances of approximately 0.1%, which is below the uncertainties for, e.g., joints in structures, as stated in Sect. 2.3.

For the steel profile, the elasticity modulus E_s, the shear modulus G_s, the Poisson ratio ν_s, and the density ρ_s as provided by [23] are utilized (Table 2). Since LVL is an orthotropic material, the elasticity moduli, $E_{x,0}$, $E_{y,0}$, and $E_{z,0}$, the shear moduli, $G_{xy,0}$, $G_{xz,0}$, and $G_{yz,0}$, the Poisson ratios, $\nu_{xy,0}$, $\nu_{xz,0}$, and $\nu_{yz,0}$, and the density ρ_0 as given by the manufacturer [24] are used (Table 3).

Since wood is a naturally grown material, variations in the material occur. In [25], the authors state a coefficient of variation (CoV) of 0.13 for the bending modulus of elasticity for timber, which is high compared to CoV = 0.03 of the elasticity modulus of structural steel given in [25]. Hence, the LVL but not the steel material properties are assigned to be uncertain inputs. Details on how the probabilities of the LVL material properties are obtained are given in Sect. 2.2.

Table 2 Steel material properties [23]

E_s [N/m^2]	G_s [N/m^2]	ν_s [-]	ρ_s [kg/m^3]
$2.1 \cdot 10^{11}$	$8.1 \cdot 10^{11}$	0.3	7850

Table 3 LVL material properties θ_0 [24]

$E_{x,0}$ [N/m^2]	$E_{y,0}$ [N/m^2]	$E_{z,0}$ [N/m^2]	$G_{xy,0}$ [N/m^2]	$G_{xz,0}$ [N/m^2]	$G_{yz,0}$ [N/m^2]	$\nu_{xy,0}$ [-]	$\nu_{xz,0}$[-]	$\nu_{yz,0}$ [-]	ρ_0 [kg/m^3]
$1.06 \cdot 10^{10}$	$2.50 \cdot 10^{9}$	$3.00 \cdot 10^{8}$	$6.00 \cdot 10^{8}$	$1.50 \cdot 10^{8}$	$1.50 \cdot 10^{8}$	0.59	0.59	0.36	530

2.2 Inverse characterization of LVL material properties by Bayesian inference

The characterization of uncertain timber material properties is done using Bayesian inference, since the method provides a good framework for such an identification. This approach is described in more detail in the following section.

The probabilities for the uncertain LVL material input parameters of the simulation model for the hybrid steel–timber structure are identified by Bayesian inference. In this method, prior information on the probability of the model parameters, i.e., the material properties of the LVL, is updated by incorporating experimentally measured data to strengthen the degree of belief in the probability of the material parameters.

The probability model of the uncertain material parameters, i.e., the posterior probabilities $p(\boldsymbol{\theta}|\mathbf{f}_{\text{exp}})$, is fitted employing Bayes' rule [26]

$$p(\boldsymbol{\theta}|\mathbf{f}_{\text{exp}}) \propto p(\mathbf{f}_{\text{exp}}|\boldsymbol{\theta})p(\boldsymbol{\theta}), \tag{1}$$

with the uncertain parameters $\boldsymbol{\theta}$, the measured data $\mathbf{f}_{\text{exp}}$, the prior probabilities of uncertain parameters $p(\boldsymbol{\theta})$, and the likelihood $p(\mathbf{f}_{\text{exp}}|\boldsymbol{\theta})$. The denominator in Bayes' formula only normalizes the probabilities, which is why it is omitted here [26]. The measured data $\mathbf{f}_{\text{exp}}$ are represented by seven natural frequencies determined from vibrational experiments on timber panels made of LVL $\mathbf{f}_{\text{exp},t}$ via experimental modal analysis. The uncertain material parameters $\boldsymbol{\theta}$ constitute the inputs to the used forward model $\mathbf{f}_t(\boldsymbol{\theta})$, which is based on a Rayleigh–Ritz approach (Sect. 2.2.3). The forward model is utilized together with the measurement data to evaluate the likelihood (Sect. 2.2.1).

2.2.1 Likelihood

The likelihood $p(\mathbf{f}_{\text{exp},t}|\boldsymbol{\theta})$ is combined with the prior probabilities $p(\boldsymbol{\theta})$ to explore the posterior densities given the measurement data $\mathbf{f}_{\text{exp},t}$. Hence, it evaluates the probability that a certain measurement is obtained given a specific material parameterization $\boldsymbol{\theta}$. The mean of the distribution represents the de facto measured natural frequencies $\mathbf{f}_{\text{exp},t}$, and the standard deviation relates to the measurement noise. The likelihood function is computed by maximizing the entropy and considering it for discrete variables by means of a residual error $\epsilon_i = f_{\text{exp},t,i} - f_{t,i}(\boldsymbol{\theta})$ [27]

$$p(\epsilon_i|\boldsymbol{\theta}, \mathbf{f}_t(\boldsymbol{\theta}), \sigma_{\text{lik},i}, \mu_{\text{lik}} = 0) = \frac{1}{\sqrt{2\pi}\sigma_{\text{lik},i}} \exp\left(- \frac{\epsilon_i^2}{2\sigma_{\text{lik},i}^2} \right), \tag{2}$$

where $f_{\text{exp},i}$ represents one of the $1 \leq i \leq N_f$ measured datasets. The used forward model $\mathbf{f}_t(\boldsymbol{\theta})$ should be able to reproduce the experimental data well.

The probability regarding each data point equals the probability of the residual error at each data point. Hence, the overall likelihood function is computed as the joint probability of all data points [27]

$$\begin{aligned} &p(\mathbf{f}_{\text{exp},t}|\boldsymbol{\theta}, f_t(\boldsymbol{\theta}), \sigma_{\text{lik},1}, \sigma_{\text{lik},2}, ..., \sigma_{\text{lik},N_f}) \\ &= p(\epsilon_1, \epsilon_2, ..., \epsilon_{N_f}|\boldsymbol{\theta}, \mathbf{f}_t(\boldsymbol{\theta}), \sigma_{\text{lik},1}, \sigma_{\text{lik},2}, ..., \sigma_{\text{lik},N_f}). \end{aligned} \tag{3}$$

Since the noise is the same for each measurement in most experiments, it is assumed that $\sigma_{\text{lik}} = \sigma_{\text{lik},i}$ for all $1 \leq i \leq N_f$. $N_f = 7$ represents the number of measured frequencies. Furthermore, as justified by the principle of maximum entropy, the individual measurements are logically independent, which leads to the joint probability as [27]

$$p(\mathbf{f}_{\text{exp},t}|\boldsymbol{\theta}, f_t(\boldsymbol{\theta}), \sigma_{\text{lik}}) = \prod_i^{N_f} \frac{1}{\sqrt{2\pi}\sigma_{\text{lik}}} \exp\left(- \frac{\epsilon_i^2}{2\sigma_{\text{lik}}^2} \right). \tag{4}$$

Additionally, to consider the repeatability of the measurements, 12 specimens $N_r = 12$ are investigated. Consequently, the scalar values in the residual error $\boldsymbol{\epsilon}_i = \mathbf{f}_{\text{exp},t,i} - \mathbf{f}_{t,i}(\boldsymbol{\theta})$ become vectors with the length N_r.

Since the hyperparameter σ_{lik} is not of particular interest in this study, marginalization is used on the joint probability to compute a likelihood probability without the standard deviation σ_{lik} [27]

$$\begin{aligned} p(\mathbf{f}_{\text{exp},t}|\boldsymbol{\theta}, \mathbf{f}_t(\boldsymbol{\theta})) &= \int p(\mathbf{f}_{\text{exp},t}, \sigma_{\text{lik}}|\boldsymbol{\theta}, \mathbf{f}_t(\boldsymbol{\theta}))d\sigma_{\text{lik}} \\ &= \int p(\mathbf{f}_{\text{exp},t}|\boldsymbol{\theta}, \mathbf{f}_t(\boldsymbol{\theta}), \sigma_{\text{lik}})p(\sigma_{\text{lik}}|\boldsymbol{\theta}, \mathbf{f}_t(\boldsymbol{\theta}))d\sigma_{\text{lik}}. \end{aligned} \tag{5}$$

Using the principle of maximum entropy, the Jeffreys' prior is assigned for the marginal distribution $p(\sigma_{\text{lik}}|\boldsymbol{\theta}, \mathbf{f}_t(\boldsymbol{\theta}))$ [27]

$$p(\sigma_{\text{lik}}|\boldsymbol{\theta}, \mathbf{f}_t(\boldsymbol{\theta})) = \frac{1}{\sigma_{\text{lik}}}. \tag{6}$$

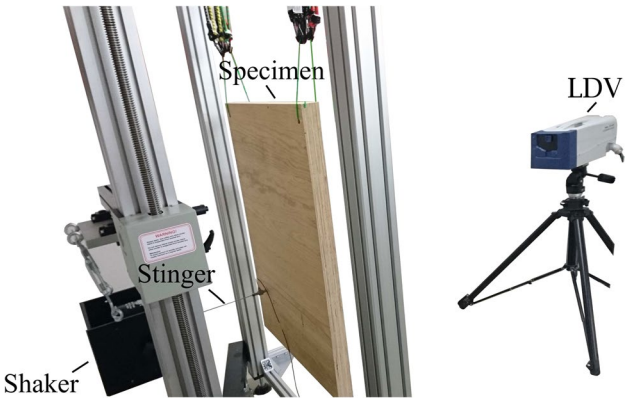

Fig. 4 Measurement setup for the components

Table 4 Dimensions of LVL samples

Label	Thickness h_t [m]	Width b_t [m]	Length l_t [m]
H451-H454	0.045	0.825	0.6
H551-H554	0.055	0.840	0.6
H651-H654	0.065	0.750	0.6

Subsequently, the integral from Eq. (5) is performed using the limits $\sigma_{\text{lik}} \in [0, \infty)$ resulting in a marginalized likelihood in the form of a student's t-distribution

$$p(\mathbf{f}_{\text{exp},t}|\boldsymbol{\theta}, \mathbf{f}_t(\boldsymbol{\theta})) = \frac{\Gamma(N_f/2)}{2}\left(\pi \sum_{i=1}^{N_f} \epsilon_i^2\right)^{-N_f/2}, \tag{7}$$

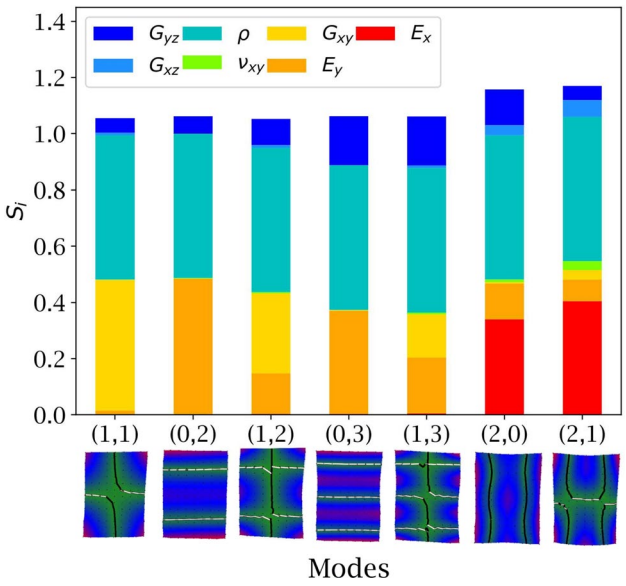

Fig. 5 Sensitivities S_i for an LVL plate with thickness $h = 4.5$ cm for the seven lowest eigenfrequencies

with the standard gamma function $\Gamma(...)$. The individual specimens' experiments are taken into account by summing the error also w.r.t. those data points

$$p(\mathbf{f}_{\text{exp},t}|\boldsymbol{\theta}, \mathbf{f}_t(\boldsymbol{\theta})) = \frac{\Gamma(N_f/2)}{2}\left(\pi \sum_{i=1}^{N_f}\sum_{j=1}^{N_r} \epsilon_{ji}^2\right)^{-N_f/2}, \tag{8}$$

where $\epsilon_{ji} = f_{\text{exp},t,ji} - f_{t,ji}(\boldsymbol{\theta})$.

2.2.2 Vibration measurements on timber panels

The experimental data are acquired by performing vibration measurements on the individual components, i.e., 12 LVL panels ($N_r = 12$). The components' measurements are established similarly to the experiments on the hybrid element (Sect. 2.1.1). A white-noise excitation is applied to the structure by the stinger. Furthermore, the sample is supported by rubber slings. The respective test setup is visualized in Fig. 4.

The first seven eigenfrequencies $f_{\text{exp},t}$ of the 12 LVL plates are identified by an experimental modal analysis [18] and are visualized below the abscissa in Fig. 5. The dimensions of the samples, i.e., length l_t, width b_t, and thickness h_t, are given in Table 4. Four samples of three different geometries are used in the experiments, i.e., H45i with a thickness of $h_t = 45$ mm, H55i with a thickness of $h_t = 55$ mm, and H65i with a thickness of $h_t = 65$ mm. The fiber direction of the LVL is aligned with the shorter side length l_t.

2.2.3 Forward model: Rayleigh–Ritz approach

A forward model is necessary to evaluate the likelihood. Here, many evaluations are required, which is why, instead of an FE approach, a computationally faster model is used. Due to its anatomy, wood is often modeled as an orthotropic material. Hence, a Rayleigh–Ritz method for orthotropic Mindlin plates with free supports is implemented [28]. In the Rayleigh–Ritz method, energy functionals for the strain and kinetic energy of the plate are calculated by considering the constitutive equations of an orthotropic Mindlin plate (details are given in the appendix). To satisfy the boundary conditions, the following trigonometric basis functions:

$$\phi_m(x) = \begin{cases} \cos(\lambda_m x) & m \geq 0 \\ \sin(\lambda_m x) & m < 0 \end{cases} \quad \lambda_m = m\pi/l_t \tag{9}$$

$$\phi_n(y) = \begin{cases} \cos(\lambda_n y) & n \geq 0 \\ \sin(\lambda_n y) & n < 0 \end{cases} \quad \lambda_n = n\pi/b_t \tag{10}$$

are utilized to describe the displacements w and rotations ψ_i of the plates

$$\psi_x(x,y) = \sum_{m=-2}^{\infty}\sum_{n=-2}^{\infty} A_{mn}\phi_m(x)\phi_n(y), \tag{11}$$

$$\psi_y(x,y) = \sum_{m=-2}^{\infty}\sum_{n=-2}^{\infty} B_{mn}\phi_m(x)\phi_n(y), \tag{12}$$

$$w(x,y) = \sum_{m=-2}^{\infty}\sum_{n=-2}^{\infty} C_{mn}\phi_m(x)\phi_n(y), \tag{13}$$

while satisfying the freely supported boundary conditions [28]. The potential and kinetic energy use the respective displacement and rotation functions depending on the coefficients A_{mn}, B_{mn}, and C_{mn} to build the Lagrangian expression. This formulation is minimized by derivation with respect to the coefficients. It is summed up in matrix form as

$$(\mathbf{K} - \omega^2\mathbf{M})\mathbf{E} = 0 \tag{14}$$

with the stiffness matrix $\mathbf{K}$, the mass matrix $\mathbf{M}$, the natural frequencies $\mathbf{f} = \boldsymbol{\omega}/(2\pi)$, and the coefficient matrix $\mathbf{E}$

$$\mathbf{E} = \begin{Bmatrix} A_{-2,-2} & A_{-2,-1} & \dots & A_{M,N} \\ B_{-2,-2} & B_{-2,-1} & \dots & B_{M,N} \\ C_{-2,-2} & C_{-2,-1} & \dots & C_{M,N} \end{Bmatrix}^T, \tag{15}$$

with truncation order $M = 8$ and $N = 8$.

From Eq. (14), natural frequencies and eigenvectors can be computed by solving the eigenproblem.

The supports of the model are chosen as 'free', similar to the freely suspended specimens in the experiments. As input parameters to the model, the dimensions of the LVL plates (Table 4) and the timber material properties $\hat{\theta}$, i.e., elasticity moduli in longitudinal E_x and transverse direction E_y, shear moduli G_{xy}, G_{xz}, and G_{yz}, density ρ and Poisson's ratio ν_{xy} are required. Using the model (Eq. (14)), natural frequencies $\mathbf{f}_{\boldsymbol{\theta}} = \mathbf{f}_t(\boldsymbol{\theta})$ are determined numerically and incorporated in the Bayesian inference.

However, first, a one-at-a-time sensitivity analysis [29, 30] is conducted to reduce the parameter space by identifying the most relevant input LVL material parameters for the Bayesian inference approach. Hence, it is evaluated which material properties mostly influence the seven lowest natural frequencies, which lie in the range of $f_{\theta_i} \in [0, 800]$ Hz. The Rayleigh–Ritz model uses seven material input parameters, i.e., the material properties. Each material property is varied in the range of $\hat{\theta}_i \in [0.9 \cdot \theta_{i,0}, 1.1 \cdot \theta_{i,0}]$. Here, $\hat{\boldsymbol{\theta}}_0 = [E_{x,0}, E_{y,0}, G_{xy,0}, G_{xz,0}, G_{yz}, \nu_{xy,0}, \rho_0]^T$ denotes the initial parameter values of the timber material properties as given in Table 3.

The variation range is chosen as ±10%, since the CoV for wooden materials is approximately given as CoV ≈ 0.1 in [25], which covers the parameter range within one standard deviation. The varied material properties are introduced in the forward model. Eigenfrequencies $\mathbf{f}_{\theta_i}$ are subsequently computed and compared to the initial results $\mathbf{f}_{\theta_0}$ obtained through the initial values $\boldsymbol{\theta}_0$. The respective modes are denoted by the number of nodal lines in the x (fiber direction) and y (transverse to the fiber) directions, e.g., (1,1), as depicted in Fig. 5. Then, the sensitivity is calculated as

$$S_i = \boldsymbol{\Delta}_f / \Delta_{\hat{\theta}} = (\mathbf{f}_{\hat{\theta}_i} - \mathbf{f}_{\hat{\theta}_0})/(\hat{\theta}_i - \hat{\theta}_0). \tag{16}$$

This yields high sensitivities ($S_i \geq 0.05$) of the natural frequencies to all input material parameters $\hat{\boldsymbol{\theta}}$ except for the Poisson's ratio ν_{xy} and the shear modulus G_{xz} (Fig. 5). Consequently, the most relevant material input parameters are identified as $\boldsymbol{\theta} = [E_x, E_y, G_{xy}, G_{yz}, \rho]^T$ and are subsequently used for the inference of the timber material properties.

2.2.4 Prior probabilities

The initial probabilities—the priors—represent the beliefs about the uncertain parameters before measurement data are considered [26]. Based on the information given in [25], lognormal distributions $\theta_i \sim \mathcal{LN}(\mu_i, \sigma_i^2)$ are assigned for the elasticity moduli, E_x and E_y, and for the shear moduli, G_{xy} and G_{yz}, and a normal distribution $\rho \sim \mathcal{N}(\mu_\rho\, \sigma_\rho^2)$ is assigned for the density ρ. μ_i denotes the location parameter in the lognormal distributions and the mean value for the normal distribution. σ_i represents the standard deviation in both cases. In [25], information on the CoV is also given as $\mathrm{CoV}_\rho = 0.1$ and $\mathrm{CoV}_{\mathrm{moduli}} = 0.13$ leading to standard deviations of $\sigma_\rho = 0.1 \cdot \rho_0$ and $\sigma_i = 0.13$. By means of the prior probabilities, prior predictive checks are performed [31]. Samples for the material values are drawn from the prior probabilities for a specific set of μ_i and σ_i, inserted into the forward model, and the seven lowest natural frequencies $\mathbf{f}_\theta$ are determined. Then, the measured natural frequencies $\mathbf{f}_{\mathrm{exp},t}$ are plotted together with the calculated natural frequencies $\mathbf{f}_\theta$. If the measured ones lie within the range spanned by the calculated values, the parameters of the prior probabilities indicate physically meaningful results for the natural frequencies. Nevertheless, for this set of standard deviations of the priors, the prior predictive checks showed measured frequencies lying outside the range of calculated values. Hence, a larger $\mathrm{CoV}_{\mathrm{moduli}} = 0.25$ than proposed for the moduli in [25] is chosen. The chosen value stems from the CoV given in [25] for the bending strength, since the moduli are related to bending strength. For this selected configuration

$$E_x \sim \mathcal{LN}(\ln(E_{x,0}),\, 0.25^2), \tag{17}$$

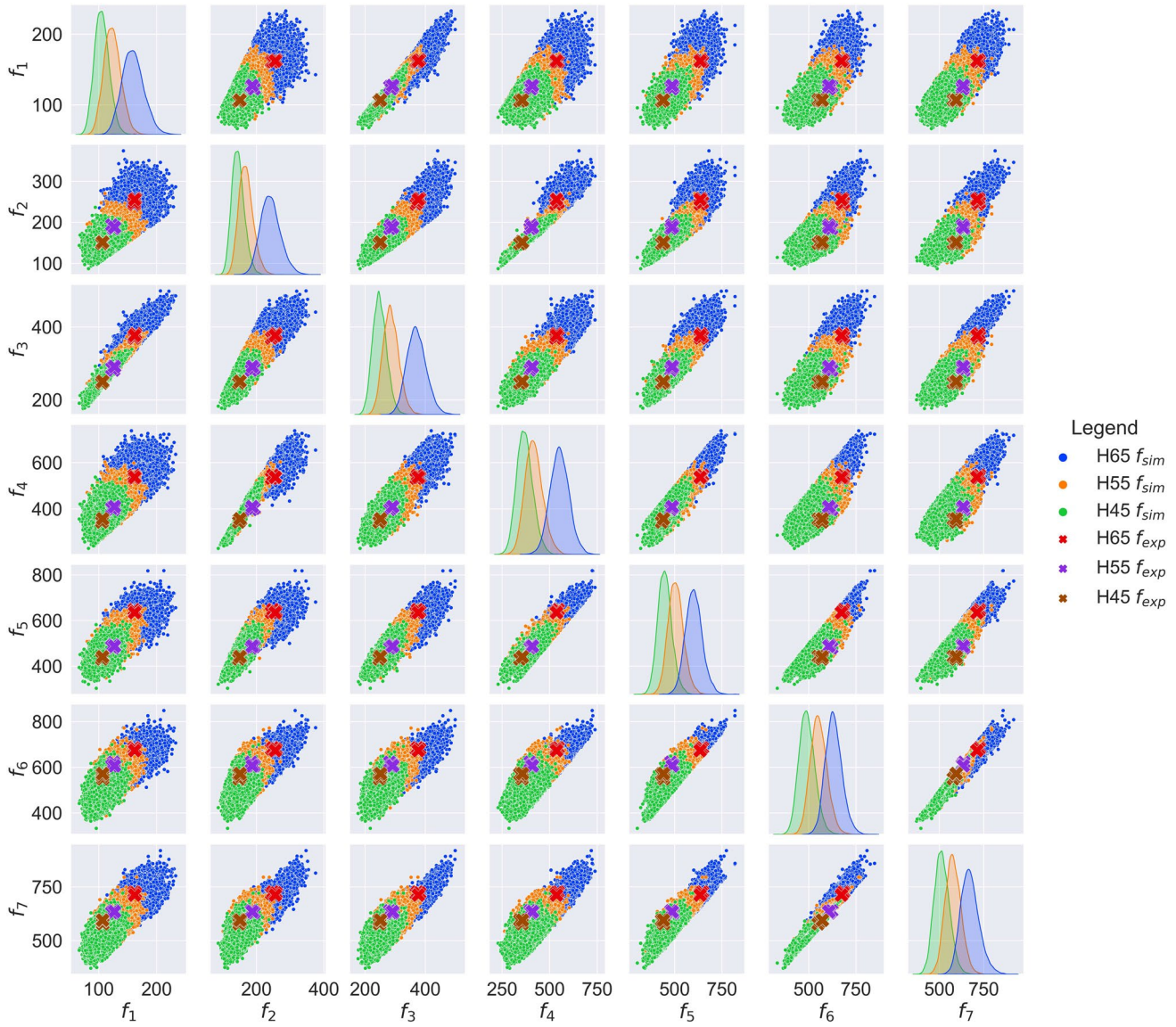

Fig. 6 Prior predictive checks: the numerically $\mathbf{f}_{\text{fem},t}$ and experimentally $\mathbf{f}_{\text{exp},t}$ determined natural frequencies are plotted using contrasting colors for the sake of comparison

$$E_y \sim \mathcal{LN}(\ln(E_{y,0}), 0.25^2), \tag{18}$$

$$G_{xy} \sim \mathcal{LN}(\ln(G_{xy,0}), 0.25^2), \tag{19}$$

$$G_{yz} \sim \mathcal{LN}(\ln(G_{yz,0}), 0.25^2), \tag{20}$$

$$\rho \sim \mathcal{N}(\rho_0, (0.10 \cdot \rho_0)^2), \tag{21}$$

the prior predictive check results are shown in Fig. 6.

All measured eigenfrequencies $\mathbf{f}_{\text{exp},t}$ lie within the range of the numerically evaluated eigenfrequencies $\mathbf{f}_\theta$. Hence, the above priors are assigned.

2.2.5 Posterior distribution

Finally, methods are needed that explore the posterior probabilities. In this context, Markov Chain Monte Carlo Sampling methods are often used, since an analytical solution only exists in rare cases, e.g., if conjugacy is present. The sampling utilizes the forward model (Sect. 2.2.3), which must be computed for each likelihood evaluation during sampling [26].

This study uses the so-called Sequential Monte Carlo sampler within the Python package PyMC [32] to infer the posterior probabilities of the uncertain material parameters θ. This algorithm is advantageous for multimodal posterior probabilities. Unlike usual Markov

Chains, the sampler is less susceptible to getting stuck in local minima, which is overcome by applying the idea of tempering [33].

The identified probability densities are subsequently available as inputs for the probabilistic analysis of the hybrid building element together with the uncertain joint stiffness values.

2.3 Uncertain joint inputs

For the modal analysis of the hybrid structure, stiffness properties for the fastener model (Fig. 3 on the right) are required. The linear spring element is applied to connect DOFs in the x- and y-direction with the stiffness k_{hor} and in the z-direction with the stiffness k_{ver}. Since different fastener types, i.e., nails[3] and screws,[4] are used for the upper and lower joint due to manufacturing reasons, different stiffness values are applied for the upper, $k_{\text{ver,u}}$ and $k_{\text{hor,u}}$, and lower, $k_{\text{ver,l}}$ and $k_{\text{hor,l}}$, joints.

Ibrahim and Pettit [34] provide an extensive overview of uncertainties in bolted joints and other fasteners. The authors point out that deterministic response evaluations could lead to unnecessarily conservative system designs, emphasizing the need to consider parameter uncertainties in jointed structures. Consequently, the joints' stiffness values are assigned to be uncertain inputs in this study.

Various studies state coefficients of variation CoV for the stiffness in joints. The identified CoV in the literature ranges from 5% [35] to 25% [36]. Subsequently, CoV = 25% is chosen for the normally distributed probabilities of the joints' stiffness. However, the joints' stiffness values are not known in advance. Hence, an MAP estimation [26, 37] approximates the mean value of the joints' stiffness. The MAP estimation is used instead of a full Bayesian inference, since the necessary large number of evaluations of the hybrid structure's FE model would require too high computational effort. MAP estimation is performed using the equations of Sect. 2.2 while replacing the forward model of the LVL plates with the FE simulation of the hybrid structure. Furthermore, the measurement data of the LVL plates are substituted by the results from the experiments on the hybrid specimen described in Sect. 2.1.1. Finally, the MAP estimation leads to the stiffness values in Table 5.

The identified values lie within a reasonable range with values given by [38], i.e., axial and shear stiffness properties of approximately 50 MPa for a beam structure jointed by M10 bolts and nuts.

[3] Unpublished prototype.

[4] Thin sheet metal screws 6.0x90 by Reisser-Schraubentechnik GmbH, D-74653 Ingelfingen-Criesbach, Germany.

2.4 Probabilistic analysis of the hybrid steel–timber building element

Utilizing the identified uncertain inputs, numerical probabilistic analysis for the modal properties of the hybrid steel–timber structure is performed to assess the influence of input uncertainties of the prediction tool. Parameter uncertainties are considered by assuming probability distributions for the inputs [26] and performing an MC simulation [39]. Here, random samples are drawn to compute the natural frequencies of the hybrid element numerically (see, e.g., [39]). Utilizing the MC method, target statistics, i.e., mean values, standard deviations, and percentiles of natural frequencies of the hybrid structure, are estimated by a set of generated realizations computed based on the samples. Latin hypercube sampling (LHS) reduces the realizations necessary for reasonable results by evenly spreading the samples over the entire sampling space [40]. In [11], LHS for MC simulations is investigated for a wooden floor model. The authors concluded that LHS using $n_{\text{LHS}} = 40$ sampling steps led to converged results for four sampled parameters. This indicates that if the number of samples n_{LHS} is chosen equal to ten times the dimension d of the parameters $n_{\text{LHS}} = 10 \cdot d$, satisfying results can be achieved. The probabilistic prediction tool used in this study is based on the model of Sect. 2.1.2 to determine the influence of model parameter uncertainties on the modal properties of the building element. Thus input uncertainties, i.e., for the LVL material properties (Sect. 2.2), E_x, E_y, G_{xy}, G_{yz} and ρ, and for the joint stiffness values, $k_{\text{ver,u}}$, $k_{\text{ver,l}}$, $k_{\text{hor,u}}$, and k_{horl} (Sect. 2.1.2), are propagated through the simulation model to the resulting natural frequencies $\mathbf{f}_{\text{FE}}$ of the hybrid steel–timber test sample.

3 Results

As uncertain LVL material properties are required for the probabilistic analysis of the hybrid steel–timber element, results concerning the Bayesian inference of the LVL's material parameters are presented first. Second, the outcomes of the probabilistic analysis of the hybrid steel–timber element are displayed.

3.1 Stochastic estimates of the material properties of the LVL

The posterior probabilities of the LVL's material properties result from the Bayesian approach (Sect. 2.2) using a Sequential Monte Carlo Sampler with seven chains, including 500 samples each. The outcome is described by the mean values $\hat{\mu}_{\theta_i}$ and the standard deviations $\hat{\sigma}_{\theta_i}$. The mean values are compared to the material parameters

Table 5 Mean values of stiffness of upper (u) and lower (l) joints in vertical (ver) and horizontal (hor) directions

$k_{\text{hor,l}}$ [N/m]	$k_{\text{hor,u}}$ [N/m]	$k_{\text{ver,l}}$ [N/m]	$k_{\text{ver,u}}$ [N/m]
$8.96 \cdot 10^6$	$8.41 \cdot 10^6$	$9.60 \cdot 10^6$	$8.86 \cdot 10^6$

provided by the manufacturer (Table 3) through the deviation of the resulting mean and the provided property $a = 1 - \hat{\mu}_{\theta_i}/\theta_{i,0}$. These results as well as the $\hat{\text{CoV}} = \hat{\sigma}_{\theta_i}/\hat{\mu}_{\theta_i}$ are listed in Table 6. Deviations above ±10% are marked in bold letters.

The difference between inferred and provided material properties lies above 5% for all parameters, often even above 10%, which represents a significant difference emphasizing the relevance of the Bayesian inference. Moreover, the identified posterior probabilities become slightly narrower than the priors for E_x, E_y, G_{xy}, and ρ, which is shown by the smaller $\hat{\text{CoV}}$ (Table 6) of these material parameters compared to the priors' CoV for the density $\text{CoV}_\rho = 0.10$ and for all other material parameters $\text{CoV}_{\theta_i} = 0.25$. The prior and posterior probabilities of all material parameters are plotted together in Fig. 7 to check the identified properties. Here, the narrower posterior probabilities are also visible. Furthermore, for all properties, the prior and posterior probabilities overlap.

Moreover, model validation is performed concerning LVL plate natural frequencies using the forward model (Sect. 2.2.3) and experimentally determined natural frequencies $\mathbf{f}_{\text{exp},t}$ of the LVL components. For this purpose, natural frequencies of the LVL panels, i.e., $H45i$, $H55i$, and $H65i$, are calculated numerically using an MC simulation (Sect. 2.4), LHS, and 6000 samples for the material properties drawn from the posterior distribution. The computed values f_i are presented in Fig. 8 as box plots together with the experimentally identified values $f_{\text{exp},t,i}$.

All measured eigenfrequencies lie within the whiskers spanned by the sampled eigenfrequencies or even within the first-to-third quartile values. Hence, the inferred material properties, together with the forward model, represent the LVL material properly.

3.2 Probabilistic modal analysis of hybrid steel–timber structure

The material properties in terms of mean and standard deviation identified before (Table 6) are used in this section, together with the parameters for the joint stiffness (Table 5), in a stochastic analysis of the hybrid steel–timber building element. Nine parameters are assigned to be uncertain and are consequently sampled from their distribution by LHS: E_x, E_y, G_{xy}, G_{yz}, ρ, $k_{\text{hor,l}}$, $k_{\text{hor,u}}$, $k_{\text{ver,l}}$, and $k_{\text{ver,u}}$. Using ten times the dimension of the parameters, the number of samples yields as $n_{\text{LHS}} = 90$. However, to verify the convergence of the results, additional samples are computed, and the results of $n_{\text{LHS}} = 110$ and $n_{\text{LHS}} = 90$ are compared. The comparison is made for the first structural eigenfrequency of the FE model at approximately $f_{\text{FE,hyb}} = 59.4\,\text{Hz}$. The following differences between the two cases are calculated:

- Deviation for mean value: $(1 - f_{\mu,110}/f_{\mu,90}) \cdot 100 = -0.1\%$.
- Deviation for standard deviation: $(1 - f_{\sigma,110}/f_{\sigma,90}) \cdot 100 = -2.8\%$.
- Deviation for 5th percentile: $(1 - f_{5\%,110}/f_{5\%,90}) \cdot 100 = -0.0\%$.
- Deviation for 95th percentile: $(1 - f_{95\%,110}/f_{95\%,90}) \cdot 100 = -0.2\%$.

Hence, the deviations lie below 1% for all evaluated stochastic parameters except for the standard deviation, which lies below 3%. This is assumed to be suitable as it is done similarly in [11, 41].

Table 7 shows the mean values f_μ, standard deviations f_σ, 5^{th} $f_{\text{P=(0.05)}}$, and 95^{th} percentile $f_{\text{P=(0.95)}}$ of the MC simulated results $f_{\text{LHS,hyb}}$ sampled by LHS with $n_{\text{LHS}} = 90$ together with the measured $f_{\text{exp,hyb}}$ and simulated eigenfrequencies f_{hyb,θ_0} using the initial material properties θ_0 (Table 3) and the joint stiffness values from Table 5. The mean values of $f_{\text{LHS,hyb}}$ differ from f_{hyb,θ_0} due to the deviating material properties identified by Bayesian inference. The identified modes, (1,1), (2,0), (2,1), (3,0), and (0,2), are named similarly to the LVL plates in Fig. 5. For a visual illustration, the plots of Fig. 5 can be considered, since the mode shapes are just scaled to a larger geometry for the hybrid structure.

Table 6 Mean values $\hat{\mu}_{\theta_i}$, the $\hat{\text{CoV}}$, the manufacturer's data $\theta_{i,0}$, and the deviation a are listed. Deviations above ±10% are marked in bold letters

	$\hat{\mu}_{\theta_i}$	$\hat{\text{CoV}}$	a	θ_0
$E_x/10^{10}\,\text{N/m}^2$	1.49	0.19	**− 0.41**	1.06
$E_y/10^9\,\text{N/m}^2$	2.27	0.18	0.09	2.50
$G_{xy}/10^8\,\text{N/m}^2$	6.86	0.21	**− 0.14**	6.00
$\rho\,\text{kg/m}^3$	496	0.08	0.06	530
$G_{yz}/10^8\,\text{N/m}^2$	1.28	0.26	**0.15**	1.50

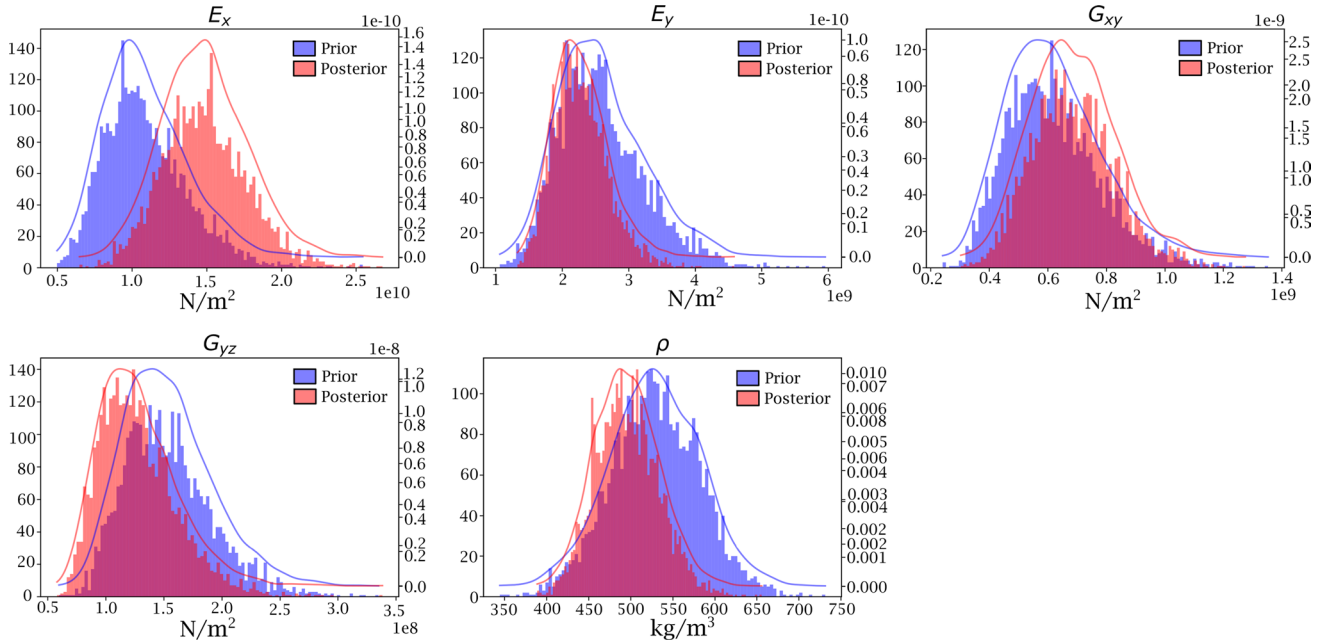

Fig. 7 Probability densities of the inferred material properties—priors (blue) and posteriors averaged for all chains (rose)

However, it has to be noted that the fiber direction of the LVL panels is oriented along its shorter edge, whereas for the hybrid panels, the fiber direction follows the long side of the panel. Hence, for the hybrid structure, the first bending mode occurs along this long side, whereas for the LVL plates, it occurs along the transversal direction. In the case of the first mode, (1,1), the mean value of $f_{\mu,\mathrm{LHS,hyb,(1,1)}}$ is close to the measured eigenfrequency $f_{\mathrm{exp,hyb,(1,1)}} = 57.1$ Hz. Hence, the calculated difference equals

$$\Delta_{\mu,\mathrm{LHS,(1,1)-exp,(1,1)}} = 2.3\,\mathrm{Hz}. \tag{22}$$

Moreover, the identified CoV for the MC simulations' mean and standard deviation range between 0.4% and 2.86%.

If the 5^{th} and 95^{th} percentiles are examined, which is state of the art in the building sector [42], the difference between the respective percentile values

$$\Delta_{5^{th}-95^{th}} = f_{\mathrm{LHS,P=(0.95)}} - f_{\mathrm{LHS,P=(0.05)}} \tag{23}$$

ranges from 1.2 Hz for mode (3,0) to 7.0 Hz for mode (2,0) (Table 7).

In Fig. 9, the probability density function estimated from the samples of the first natural frequency for mode (1,1) is visualized together with the measured frequencies, and the 5^{th} and 95^{th} percentile values. Although the measured natural frequency does not perfectly match the point of maximum probability of the probability density function, it is still covered by the percentile values, showing an adequate prediction of the FE model concerning the lowest natural frequency of the hybrid element. However, the remaining measured natural frequencies $f_{\mathrm{exp,hyb}}$ (Table 7) do not lie within the percentile values computed by the MC simulation. One possible reason for the deviations in the modes (2,0), (3,0), and (2,1) is the assumption of an ideal geometry of the steel core in the FE model. In the ideal configuration, stiffness is gained via the trapezoidal slopes of the steel core. However, since these are most likely not ideally positioned in the test specimen, a stiffer structure is obtained in the simulation than in the measurement. This is reflected in the higher natural frequencies. In the case of mode (0,2), pre-deformations and residual stresses of the steel core could stiffen the test specimen as a result of the manufacturing process. Since no pre-deformations and residual stresses are considered in the model, the model behaves less stiffly than in the measurement.

4 Discussion

The statistical estimates of the LVL material properties are used in the forward model to compute the natural frequencies of LVL plates. The computed values comply well with the measured eigenfrequencies for equivalent LVL plates, which indicates physically meaningful inferred material properties. Furthermore, the inferred posterior distributions are narrower than the priors, which implies less uncertainty of the material parameters once the measurement data are taken into account.

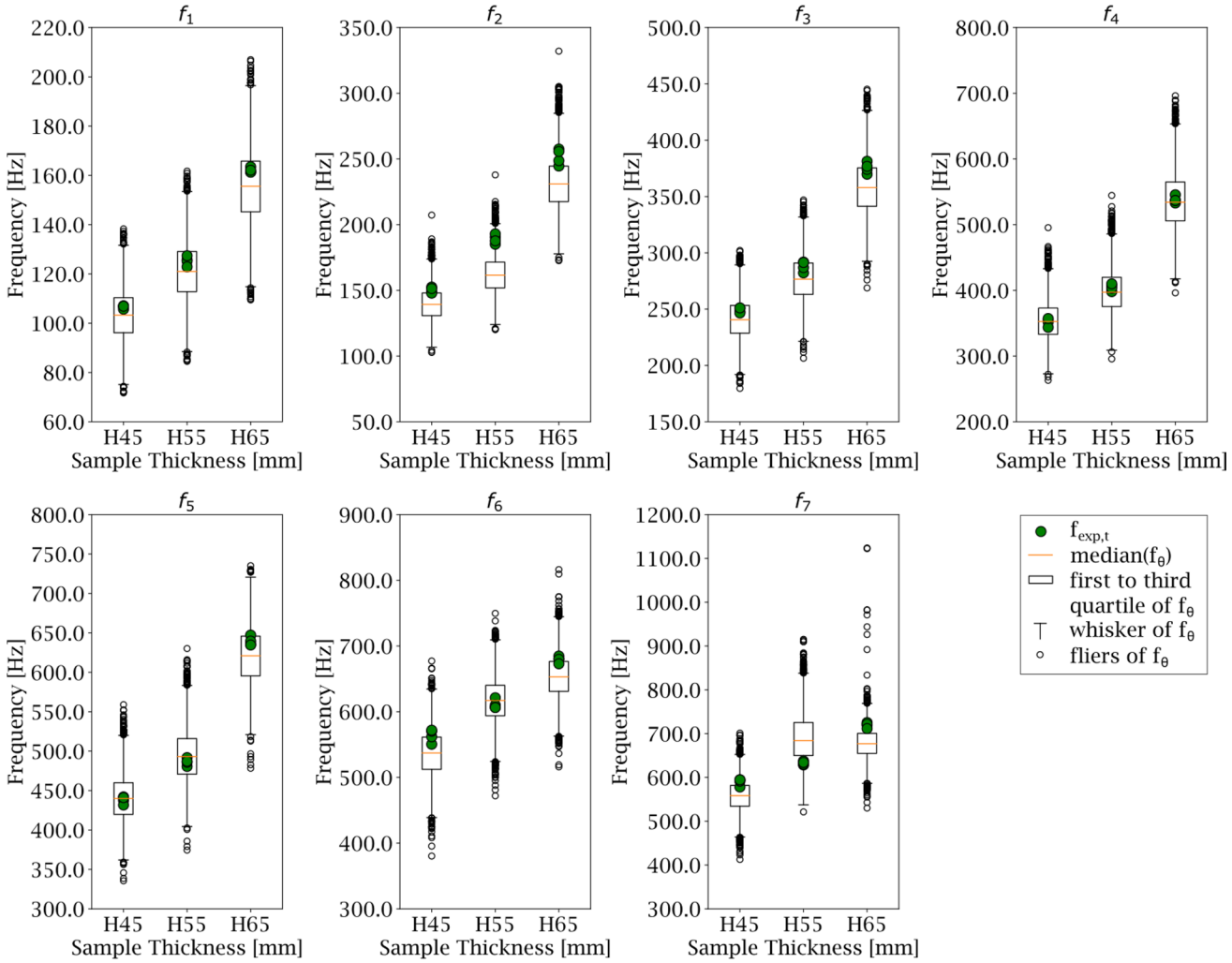

Fig. 8 Box plots of simulated eigenfrequencies of LVL plates using inferred material properties compared to experimentally determined eigenfrequencies (green markers)

The MC simulation of the hybrid steel–timber building element leads to converged results for 90 Latin Hypercube samples. The resulting statistical estimates of the natural frequencies show deviations of 5–7 Hz for some of the 5th and 95th percentiles, which represents a significant difference and, hence, should be addressed for a proper design of a structure. Moreover, the deviation of the sampled mean values for the natural frequencies differs from the computed frequencies using the initial material properties provided by the manufacturer, which emphasizes the need for material parameter identification.

The first measured eigenfrequency for mode (1,1) lies within the range spanned by the simulated eigenfrequencies, which is essential since the first eigenfrequency of a floor is relevant for a design in terms of serviceability related to vibration, e.g., in the European timber design standard [43]. Still, the MC simulation results do not cover the other experimentally identified natural frequencies. Further investigations might lead to deeper insight, e.g., considering frequency-dependent material and joint parameters or residual stresses in the hybrid element. Furthermore, an approach using Bayesian inference not only for the wooden material properties but also for the joint parameters might lead to better results. However, a faster model is required for this. Possible approaches could be surrogate models or model order reduction.

Moreover, it should be noted that, currently, no strength-related characteristics are included in the investigations. Static test series and further studies concerning, e.g., load-carrying capacity could be analyzed in future studies but are out of the scope of the current work.

Table 7 Mean values μ, standard deviation σ, 5^{th} percentile $f_{P=(0.05)}$, and 95^{th} percentile $f_{P=(0.95)}$ of eigenfrequencies $f_{\mathrm{LHS,hyb}}$, ranges between 5^{th} and 95^{th} percentile values $\Delta_{5^{th}-95^{th}}$, measured $f_{\mathrm{exp,hyb}}$ and initially simulated eigenfrequencies $f_{\mathrm{hyb},\theta_0}$ are listed

f_i [Hz]	$f_{\mathrm{LHS,hyb}}$ [Hz]				$\Delta_{5^{th}-95^{th}}$ [Hz]	$f_{\mathrm{hyb},\theta_0}$ [Hz]	$f_{\mathrm{exp,hyb}}$ [Hz]
for mode	μ	σ	$P = (0.05)$	$P = (0.95)$			
(1,1)	59.4	1.7	56.8	62.5	5.7	52.1	57.1
(2,0)	83.6	2.3	80.1	87.1	7.0	77.2	70.9
(2,1)	105.3	0.8	103.3	106.2	3.0	95.4	76.4
(3,0)	108.4	1.4	105.6	110.1	4.5	99.7	88.3
(0,2)	99.5	0.4	98.9	100.1	1.2	102.3	113.9

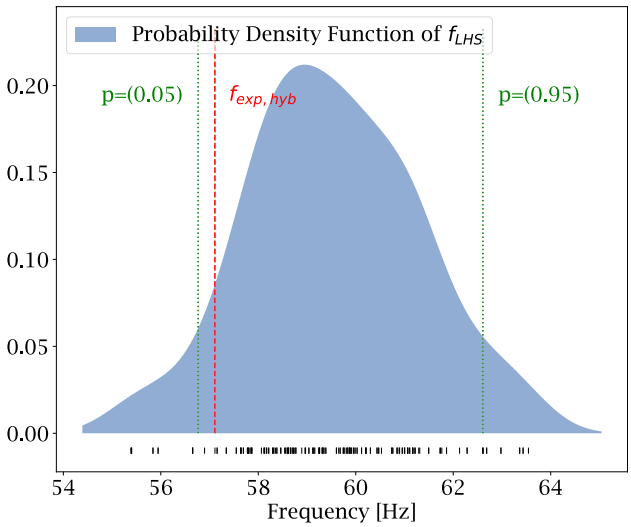

Fig. 9 Probability density function estimated by $f_{\mathrm{LHS,hyb},(1,1)}$, measured frequencies $f_{\mathrm{exp,hyb},(1,1)}$, and percentiles $P = (0.05)$ and $P = (0.95)$

5 Conclusions

In summary, this research article leverages Bayesian inference and Monte Carlo simulation to address uncertainty in the modal properties of a hybrid steel–timber building element. The primary goal of the research is to facilitate more efficient building designs by shifting from traditional conservative safety factors to an approach that accounts for data uncertainty. The hybrid building element under investigation features a structure comprising a trapezoidal steel web and laminated veneer lumber flanges. Given the inherent variability in timber materials, Bayesian inference is employed to derive probability distributions representing the timber's material properties, thereby providing a realistic representation of uncertainty. The key findings are itemized as follows:

- The posterior probabilities obtained through Bayesian inference reveal narrower probability distributions than the prior knowledge, denoting a reduction in uncertainty regarding the timber's material properties.
- The research uncovers an unexpected and substantial deviation of inferred mean values from manufacturer-provided data, emphasizing the importance of accounting for real-world variability in structural design.

The inferred material properties, together with uncertain joint parameters, are utilized in a Monte Carlo simulation. Mean values of joint properties are estimated using maximum a posteriori estimation, and the coefficient of variation is assigned based on literature data. Employing Latin hypercube sampling and a finite element model, a probabilistic analysis of the hybrid building element is performed. Here, the following outcomes are observed:

- The 5th and 95th percentiles of the structure's natural frequencies resulting from the Monte Carlo simulation span a range of up to 7 Hz for the natural frequency at 83.6 Hz. This range emphasizes the significant variability inherent in the structural response and underlines the critical necessity of considering uncertainty in the design of building elements.
- The first measured natural frequency for mode (1,1) falls within the range spanned by the simulated eigenfrequencies, which is crucial for designing a floor with consideration for vibration-related serviceability. However, it is observed that the other measured eigenfrequencies do not align with the range of eigenfrequencies calculated by the Monte Carlo simulation, suggesting the need for further investigations.

These findings collectively contribute to advancing the field of structural engineering, emphasizing the significance of probabilistic modeling and uncertainty quantification in optimizing building designs for enhanced efficiency. Future research avenues could involve extending Bayesian inference to incorporate joint parameters and exploring alternative fastener models to refine our understanding of hybrid element behavior.

Appendix

The Lagrangian for the orthotropic Mindlin plates is computed as [28]

$$L = T - U \tag{24}$$

with the strain energy U and the kinetic energy T. The strain energy is calculated as

$$\begin{aligned} U = \iint_A \Bigg\{ & D_{11}\left(\frac{\partial \psi_x}{\partial x}\right)^2 + D_{22}\left(\frac{\partial \psi_y}{\partial y}\right)^2 \\ & + (\mu_{xy} D_{11} + \mu_{yx} D_{22}) \frac{\partial \psi_x}{\partial x}\frac{\partial \psi_y}{\partial y} \\ & + D_{xy}\left(\frac{\partial \psi_x}{\partial y} + \frac{\partial \psi_y}{\partial x}\right)^2 + \kappa G_{xz} h\left(\psi_x + \frac{\partial w}{\partial x}\right)^2 \\ & + \kappa G_{yz} h\left(\frac{\partial w}{\partial y}\right)^2 \Bigg\} \mathrm{d}x\mathrm{d}y \end{aligned} \tag{25}$$

with the flexural rigidities of the plate

$$D_{11} = \frac{E_x h^3}{12(1 - \nu_{xy}\nu_{yx})}, \tag{26}$$

$$D_{12} = \frac{\nu_{xy} E_x h^3}{12(1 - \nu_{xy}\nu_{yx})}, \tag{27}$$

$$D_{21} = \frac{\nu_{yx} E_y h^3}{12(1 - \nu_{xy}\nu_{yx})}, \tag{28}$$

$$D_{22} = \frac{E_y h^3}{12(1 - \nu_{xy}\nu_{yx}^2)}, \tag{29}$$

$$D_{xy} = \frac{G_{xy} h^3}{12}. \tag{30}$$

Moreover, the total kinetic energy is given as

$$T = \frac{\rho h \omega^2}{2} \int_0^l \int_0^b [w^2 + h^2(\psi_x^2 + \psi_y^2)/12]\mathrm{d}x\mathrm{d}y. \tag{31}$$

Funding Open Access funding enabled and organized by Projekt DEAL. This study was financially supported by the German Federal Ministry of Food and Agriculture through the Fachagentur Nachwachsende Rohstoffe e.V. (FNR) (grant number 22009817). Furthermore, the authors gratefully acknowledge the help of the chair of*Timber Structures and Building Construction at Karlsruhe Institute of Technologyfor assistance with the measurements. Furthermore, the authors are thankful for the support of the manufacturers in providing the materials for the samples.*

Data availability Some or all data, models, or codes that support the findings of this study are available from the corresponding author upon reasonable request.

Declarations

Competing interests Bettina Chocholaty was financially supported by the German Federal Ministry of Food and Agriculture through the Fachagentur Nachwachsende Rohstoffe e.V. (FNR) (grant number 22009817). All authors declare that they have no conflicts of interest.

Ethical statement No experiments on animals and humans are conducted in this article. There are no human subjects in this study and informed consent is not applicable. Furthermore, critical data, such as personal information, are not analyzed.

Open Access This article is licensed under a Creative Commons Attribution 4.0 International License, which permits use, sharing, adaptation, distribution and reproduction in any medium or format, as long as you give appropriate credit to the original author(s) and the source, provide a link to the Creative Commons licence, and indicate if changes were made. The images or other third party material in this article are included in the article's Creative Commons licence, unless indicated otherwise in a credit line to the material. If material is not included in the article's Creative Commons licence and your intended use is not permitted by statutory regulation or exceeds the permitted use, you will need to obtain permission directly from the copyright holder. To view a copy of this licence, visit http://creativecommons.org/licenses/by/4.0/.

References

1. Cheraghi-Shirazi N, Crews K, Malek S. Review of Vibration Assessment Methods for Steel-Timber Composite Floors. Buildings. 2022;12(12):2061. https://doi.org/10.3390/buildings12122061.
2. Hassanieh A, Chiniforush AA, Valipour HR, Bradford MA. Vibration behaviour of steel-timber composite floors, part (2): evaluation of human-induced vibrations. J Constr Steel Res. 2019;158:156–70. https://doi.org/10.1016/j.jcsr.2019.03.026.
3. Technical Committee ISO/TC 98/SC 2. ISO 10137:2007(E) - Bases for design of structures - Serviceability of buildings and walkways against vibrations; 2007.
4. Technical Committee ISO/TC 43/SC 2. EN ISO 10140-3 - Acoustics - Laboratory measurement of sound insulation of building elements - Part 3: Measurements of impact sound insulation; 2021. https://doi.org/10.31030/3237068.
5. Chocholaty B, Roozen NB, Maeder M, Marburg S. Vibroacoustic response of steel-timber composite elements. Eng Struct. 2022;271: 114911. https://doi.org/10.1016/j.engstruct.2022.114911.
6. Chiniforush AA, Alamdari MM, Dackermann U, Valipour HR, Akbarnezhad A. Vibration behaviour of steel-timber composite floors, part (1): Experimental & numerical investigation. J Constr Steel Res. 2019;161:244–57. https://doi.org/10.1016/j.jcsr.2019.07.007.
7. Soize C. A comprehensive overview of a non-parametric probabilistic approach of model uncertainties for predictive models in structural dynamics. J Sound Vib. 2005;288(3):623–52. https://doi.org/10.1016/j.jsv.2005.07.009.
8. Brake MR. The mechanics of jointed structures. Cham: Springer; 2016.

9. Gant F, Rouch P, Champaney L. Updating of uncertain joint models using the Lack-of-Knowledge theory. Computers & Structures. 2013;128:128–35. https://doi.org/10.1016/j.compstruc.2013.06.013.
10. Qian C, Ménard S, Bard D, Negreira J. Development of a vibroacoustic stochastic finite element prediction tool for a CLT floor. Appl Sci. 2019;9(6):1106. https://doi.org/10.3390/app9061106.
11. Persson P, Flodén O. Effect of material parameter variability on vibroacoustic response in wood floors. Appl Acoust. 2019;146:38–49. https://doi.org/10.1016/j.apacoust.2018.10.034.
12. Sepahvand K, Marburg S. Identification of composite uncertain material parameters from experimental modal data. Probab Eng Mech. 2014;37:148–53. https://doi.org/10.1016/j.probengmech.2014.06.008.
13. Sepahvand K, Marburg S, Hardtke HJ. Stochastic free vibration of orthotropic plates using generalized polynomial chaos expansion. J Sound Vib. 2012;331(1):167–79. https://doi.org/10.1016/j.jsv.2011.08.012.
14. Gogu C, Haftka R, Le Riche R, Molimard J, Vautrin A, Sankar B. Bayesian statistical identification of orthotropic elastic constants accounting for measurement and modeling errors. In: 50th AIAA/ASME/ASCE/AHS/ASC Structures, Structural Dynamics, and Materials Conference 17th AIAA/ASME/AHS Adaptive Structures Conference 11th AIAA No; 2009. p. 2258. https://doi.org/10.2514/6.2009-2258.
15. Daghia F, de Miranda S, Ubertini F, Viola E. Estimation of elastic constants of thick laminated plates within a Bayesian framework. Compos Struct. 2007;80(3):461–73. https://doi.org/10.1016/j.compstruct.2006.06.030.
16. Melzerová L, Janda T, Šejnoha M, Šejnoha J. FEM models of glued laminated timber beams enhanced by Bayesian updating of elastic moduli. International Journal of Civil and Environmental Engineering. 2015;9(5):692–8.
17. Schneider F, Papaioannou I, Straub D, Winter C, Müller G. Bayesian parameter updating in linear structural dynamics with frequency transformed data using rational surrogate models. Mech Syst Signal Process. 2022;166: 108407. https://doi.org/10.1016/j.ymssp.2021.108407.
18. Ewins DJ. Modal Testing - Theory, Practice and Application. New York: John Wiley & Sons; 2009.
19. ANSYS, Inc . Ansys Engineering Simulation Software; 2019.R1. Available from: https://www.ansys.com/.
20. Shen Z, Liu X, Zang C, Hu S. Bayesian Uncertainty Identification of Model Parameters for the Jointed Structures with Nonlinearity. Shock and Vibration. 2021;2021. https://doi.org/10.1155/2021/2638995.
21. Langer P, Maeder M, Guist C, Krause M, Marburg S. More than six elements per wavelength: The practical use of structural finite element models and their accuracy in comparison with experimental results. J Comput Acoust. 2017;25(04):1750025. https://doi.org/10.1142/s0218396x17500254.
22. Ballast DK. Handbook of construction tolerances. John Wiley & Sons; 2007.
23. Andrej A. Schneider: Bautabellen für Ingenieure. vol. 21. Bundesanzeiger Verlag; 2014. https://doi.org/10.1002/best.201190039.
24. STEICO SE. Konstruktionsheft von STEICO zu LVL/Furnierschichtholz; 2020. Accessed: 2021-01-19. Available from: https://www.steico.com/de/downloads/dokumente/produkte-allgemeines.
25. Faber M, Vrouwenvelder T. JCSS PROBABILISTIC MODEL CODE - Part III: Resistance Models; 2006. Accessed: 2023-02-02. https://www.jcss-lc.org/jcss-probabilistic-model-code/.
26. Gelman A. Bayesian Data Analysis. 3rd ed. Chapman and Hall/CRC; 2013.
27. Xiang N. Model-based Bayesian analysis in acoustics-A tutorial. The Journal of the Acoustical Society of America. 2020;148(2):1101–20. https://doi.org/10.1121/10.0001731.
28. Shi D, Zhuang Z, Zhang T. Free vibration analysis of orthotropic rectangular Mindlin plates with general elastic boundary conditions. In: INTER-NOISE and NOISE-CON Congress and Conference Proceedings. vol. 249. Institute of Noise Control Engineering; 2014. p. 1477–1485.
29. Mottershead JE, Link M, Friswell MI, Schedlinski C. Model updating. Handbook of Experimental Structural Dynamics. 2020;p. 1–53.
30. Basaglia BM, Li J, Shrestha R, Crews K. Response prediction to walking-induced vibrations of a long-span timber floor. J Struct Eng. 2021;147(2):04020326. https://doi.org/10.1061/(asce)st.1943-541x.0002888.
31. Wesner JS, Pomeranz JP. Choosing priors in Bayesian ecological models by simulating from the prior predictive distribution. Ecosphere. 2021;12(9): e03739. https://doi.org/10.1101/2020.12.10.419713.
32. Salvatier J, Wiecki TV, Fonnesbeck C. Probabilistic programming in Python using PyMC3. PeerJ Computer Science. 2016;2: e55. https://doi.org/10.7717/peerj-cs.55.
33. Martin O. Bayesian Analysis with Python: Introduction to statistical modeling and probabilistic programming using PyMC3 and ArviZ. Packt Publishing Ltd; 2018.
34. Ibrahim R, Pettit C. Uncertainties and dynamic problems of bolted joints and other fasteners. J Sound Vib. 2005;279(3–5):857–936. https://doi.org/10.1016/j.jsv.2003.11.064.
35. Gangadharan SN, Nikolaidis E, Haftka RT. Probabilistic system identification of two flexible joint models. AIAA J. 1991;29(8):1319–26. https://doi.org/10.2514/6.1990-1144.
36. Segalman DJ, Gregory DL, Starr MJ, Resor BR, Jew MD, Lauffer JP, et al. Handbook on dynamics of jointed structures. Sandia National Laboratories, Albuquerque. 2009;.
37. Gauvain JL, Lee CH. Maximum a posteriori estimation for multivariate Gaussian mixture observations of Markov chains. IEEE transactions on speech and audio processing. 1994;2(2):291–8. https://doi.org/10.1109/89.279278.
38. Shah MA, Yunus M, Rani MA, Omar R, Mora A. Stochastic model updating of bolt-jointed structure for structural dynamics applications. International Journal of Automotive and Mechanical Engineering. 2021;18(2):8760–71. https://doi.org/10.15282/ijame.18.2.2021.14.0670.
39. Kroese DP, Taimre T, Botev ZI. Handbook of monte carlo methods. John Wiley & Sons; 2013.
40. Olsson AM, Sandberg GE. Latin hypercube sampling for stochastic finite element analysis. J Eng Mech. 2002;128(1):121–5. https://doi.org/10.1061/(asce)0733-9399(2002)128:1(121).
41. Luegmair M, Schmid JD. Challenges in vibroacoustic vehicle body simulation including uncertainties. SAE Technical Paper; 2020.
42. Technical Committee CEN/TC 250. DIN EN 1990:2021-10 - Eurocode: Basis of structural design - German Version; 2021.
43. Technical Committee CEN/TC 250. Eurocode 5: Design of timber structures, Part 1-1: General - Common rules and rules for buildings [Standard]; 2010.

Publisher's Note Springer Nature remains neutral with regard to jurisdictional claims in published maps and institutional affiliations.